

DESIGN CONSIDERATIONS 6H-SiC PIEZORESISTIVE ACCELEROMETERS

Cristiana VOICAN, Constantin D. STANESCU

University "Politehnica of Bucharest"

voicancristiana@yahoo.com ; prof_cstanescu@yahoo.com

Keywords: piezoresistive; accelerometers; 6H-SiC

Abstract. The results from finite element analysis (FEA) of the selected design models were compared to evaluated prototypes. While FEA results predicted safe operation above 100,000-g's, preliminary experimental tests were performed up to 40,000-g's. Sensitivities ranging between 50 and 343 nV/g were measured. Non-linear behavior was observed over the shock range relative to the commercial accelerometer used as a benchmark. These initial results offer promise for the use of 6H-SiC accelerometers for extreme impact sensing in strong EM fields and temperature up to 600⁰ C that are beyond the capability of silicon.

1. INTRODUCTION

The need for improved system performance in extreme impact (>100,000-g's), high electromagnetic (EM) fields (> 18 Tesla in some railguns), and high temperature (>500⁰ C) environments has placed strong demand for more robust instrumentation. Commercially available accelerometers based on silicon technology have been demonstrated to survive nearly 100,000-g's [2], but its material properties may inhibit reliable operation in application-desired high temperatures (>350⁰ C) unless more complex and expensive packaging schemes are adopted [5]. In addition, these accelerometers must survive the EM fields associated with the all-electric vehicle technology for military and space applications. In response to these needs, a collaborative effort between the National Aeronautics and Space Administration (NASA) Glenn Research Center, the United States Air Force Research Laboratory (AFRL) Munitions Directorate, and Cornell University has initiated work aimed at establishing the critical enabling technology infrastructure (modeling, fabrication, and validation) required for the implementation of SiC accelerometers designed specifically for extreme environments.

The choice of SiC is largely due to its excellent thermomechanical properties over silicon. Although with a relatively lower gauge factor of 30 [10] compared to silicon of about 90 [7], SiC compensates with a higher Young's modulus of approximately 448 GPa [11] compared to 129.5 GPa for (100) silicon [4]. SiC does not suffer from thermally induced plastic deformation associated with similarly designed silicon membranes when heated above 500⁰ C [6]. SiC has a melting temperature of around 2800⁰ C, compared to 1412⁰ C for silicon. In addition to its superior thermomechanical properties, single crystal SiC has a wide band gap ranging from 2.39 eV for the cubic 3C-SiC polytype to 3.2 eV for the 4H-SiC hexagonal polytype, compared to 1.12 eV for single crystal silicon. Therefore, thermal generation of carriers that results in increased reverse leakage current across the pn-junction is very minimal even at 600⁰ C.

In this initial effort, we have selected four different configurations within a design matrix and performed extensive micromechanical finite element analysis (FEA) [1] that included static, modal, and transient analyses. This was followed by sensor fabrication and evaluation. For packaging, the sensors were epoxied into

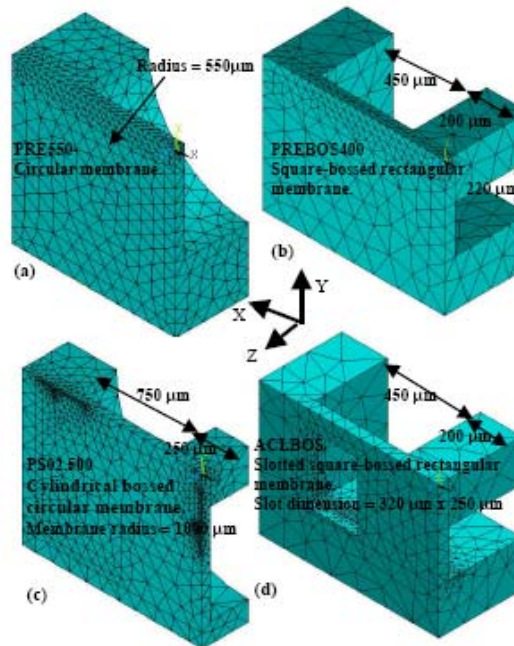


Figure 1: Mesh of quarter-symmetry model for the four 6H-SiC device configurations analyzed and tested. Membrane thickness = 60 μm .

a ceramic dualinline-pin package and aluminum wirebond was applied between the sensor and package. This un-optimized packaging used in the aggressive test environment was expected to cause significant deviation between FEA prediction and physical results. However, the interest at this initial study was to validate device survivability and worse case measurement deviation from a selected commercial-off-the-shelf accelerometer that was used as a benchmark [3]. The four designs investigated at this initial phase are described by the quarter-symmetry geometries shown in Figure 1.

2. ACCELEROMETER DESCRIPTION

The as fabricated 6H-SiC accelerometer chip sizes ranged from 4 mm² to 6.25 mm² in area, with Wheatstone bridge configured circuit. The piezoresistive mesa elements were dry-etched in (0001)-oriented n-type (doping level $3.8 \times 10^{18} \text{ cm}^{-3}$) 6H-SiC epilayer grown by chemical vapor deposition on a high resistivity (7 $\Omega\text{-cm}$) p-type 6H-SiC substrate. The scanning electron microscope of a representative ACLBOS400 configuration is shown in Figure 2a while a cross-section is shown in Figure 2b to depict the relative positions of the resistors. The four sensing elements are placed longitudinally on the narrow beams, each located on the inner edge of the peripheral rigid structure and at the opposite

edges of the centered inertial proof mass (boss). Both the front side and backside were fabricated by a deep reactive ion etching process. The two narrow beams that carry the piezoresistors transfer strain to the piezoresistors, thereby effecting a change in output voltage of the Wheatstone bridge. The wider beams can be modified during design to predetermine the strain transferred to the narrow resistor-carrying beams. The two inner piezoresistors are placed on the center boss, but because of their length, they overhang the boss edge on two sides. Ideally, such placement allows both resistors to experience similar stress, compressive or tensile, depending on the direction of the applied external stimulus. Sections of the outer piezoresistors on the narrow structural beam also overhang the inner peripheral edge of the solid section as indicated in Figure 2b. When an external stimulus is applied, the stress component of these external resistors is, ideally, equal and have the same sign, but opposite that of the inner resistors.

The design considerations for the accelerometer take into account key design parameters that are required to develop robust SiC sensors to survive extreme environments. The key design parameters considered included the safe

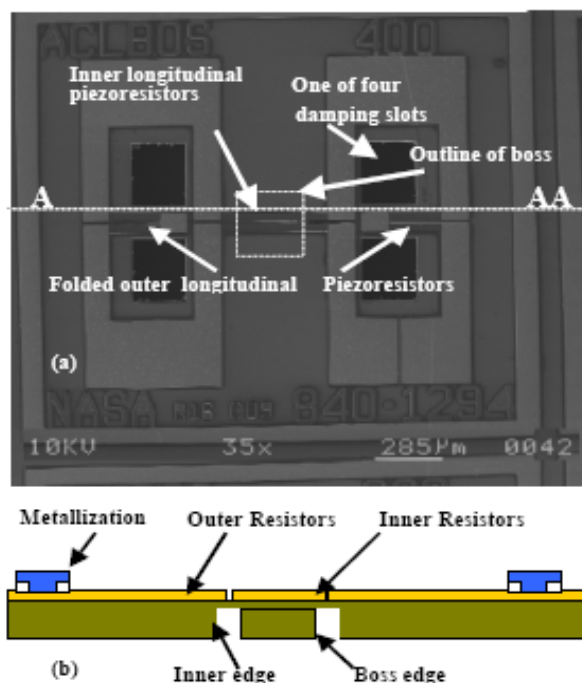


Figure 2: a) SEM micrograph of accelerometer depicts the four longitudinal piezoresistors placed on the narrow beams; b) A-AA cross section of Figure 2a depicts the relative locations of the inner and outer resistors on the narrow beams

operating stress (SOS), which took into consideration the inertial mass, diaphragm thickness and radius, and damping characteristics of the accelerometer design. In this work the maximum SOS was set at 50% of the fracture strength of SiC (450MPa) [9].

3.FINITE ELEMENT ANALYSIS

Simulations were performed to extract the behavioral parameters of the structure representing each design configuration. The FEA can analyze the distributed nature of the mass of the structure instead of the lumped mass approximation of the theory. The device geometry was either imported from the layout tool [8] or directly generated in the simulation tool where the solid geometry was cut into quarters and all but one quarter was deleted as depicted in Figure 1 to greatly reduced the analysis time. The element selected to mesh the solid geometry was SOLID187 [1] which is a higher order 3-D, 10-node element with quadratic displacement behavior and three degrees of freedom at each node: translations in the nodal x, y, and z directions. The boundary conditions were applied such that the back face (not including the boss) was fixed in all three degrees of freedom to prevent rigid body motion. Then the symmetry boundary condition was applied to the exposed quarter-symmetry faces.

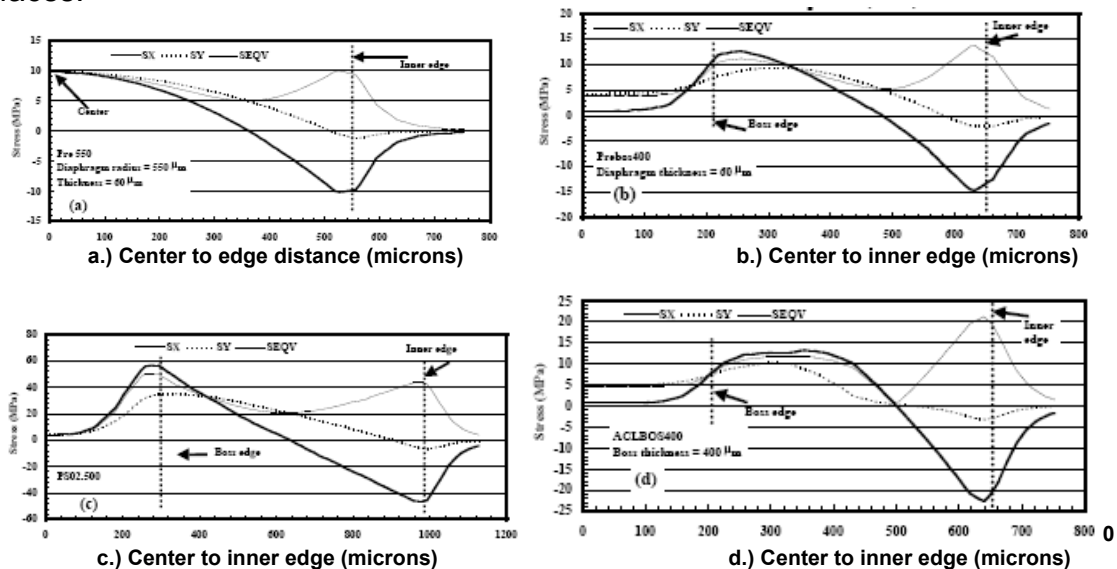


Figure 3: Static stress distribution along the x- and y-stress of the four 6H-SiC accelerometers show points of maximum tensile and compressive stress magnitudes at applied load of 100,000-g's. Note: The y-stress values are those intersecting the x-axis

The stresses in the x- (SX) and y- (SY) directions and the von Mises equivalent stress (SEQV) are shown in Figures 3 a-d for an applied acceleration of 100,000-g's. The x-axis in each plot represents the distance along the A-AA line of Figure 2a, starting from the center and moving along that line to the right edge of each structure. This is the path along which the piezoresistors are located. The stress profile of PRE550 in Figure 3a follows the usual profile for a simple circular plate that is fixed at the edge. The stress in the x-direction is compressive at the edge and becomes tensile at the center and is approximately equal in magnitude as was found in [12]. Resistors placed at these locations will experience the highest sensitivity. Since both the x- and y-axis are essentially radial and tangential on circular diaphragms, the resistors at the center location

will experience large tangential Poisson strain that adds negative piezoresistance parasitic to the measured output. In Figure 3b (PREBOS400), the maximum stress in the compressive and tensile regions is not equal. This implies unequal sensitivity between the inner and outer resistors. However, the y-axis stress component is reduced, thereby minimizing the parasitic. In Figure 3c, which has a cylindrical boss, the x-axis stress at both regions is also opposite in signs and unequal in magnitude. In this case too, the y-axis stress at the boss edge is relatively less than its corresponding x-axis stress at the same section, but the resistors will also experience unequal sensitivity. The stress profile in Figure 3d (ACLBOS400) is similar to PREBOS. Also, like PREBOS, the magnitudes of the stresses in the tensile and compressive regions are not equal. However, the stress is relatively higher at the outer edge than the PREBOS400, indicating the effect of having perforations in the diaphragm. The observed asymmetry in the stress magnitudes at the inner and outer resistors for the bossed structures is an area where geometric optimization will be needed.

REFERENCES

- [1] ANSYS Inc. 201 Johnson Road, Houston, PA 15342-1300
- [2] Brown T. G, Davis B., Hepner D., Faust J., Myers C., Muller C., Harkins T, . Holis M., and Placzankis B. , "Strap-Down Microelectromechanical (MEMS) Sensors for High-G Munition Applications,"*IEEE Trans. On Magnetics*, vol: 37 No. 1, pp. 336-342, Jan. 2001..
- [3] Endevco Corporation, 30700 Rancho Viejo Road, San Juan Capistrano, CA 92675.
- [4] Greenwood J. C., "Silicon in Mechanical Sensors," *J. Phys. E., Sci. Instrum.*, 21, pp. 1114-1128, 1988.
- [5] Katulka G. L., Hepner D. J., Davis B., Irwin E., Ridgley M., and Kornegay K., "Characterization of Silicon Carbide and Commercial-Off-The-Shelf (COTS) Components for High-g Launch and EM Applications," *IEEE Trans on Magnetics*, vol: 37 No.1, pp. 248-251, Jan. 2001
- [6] Kurtz A. D., Nunn T. A., and Weber R. A., US Patent # 4,672,354, 1987.
- [7] M. J. Madou, *The MEMS Handbook* ed. M. Gad-el-Hak, CRC Press, Boca Raton, Chapter 16, pp. 28, 2001.
- [8] MEMSCAP Inc. 180 Grand Avenue, Oakland, CA 94612
- [9] Savrun E. and Toy C., "An Aluminum Nitride Package for 600 oC and Beyond," Proceedings, 4th Intl. High Temperature Electronics Conf., Albuquerque, New Mexico, pp. 265-268, June 14-18, . 1998
- [10] Shor J. S., Bemis L., and Kurtz A. D., "Characterization of monolithic n-type 6H-SiC piezoresistive sensing elements," *IEEE Trans. Electron Devices*, vol. 41. pp. 661-665, May 1994
- [11] Silicon Carbide, eds. H. K. Henisch and R. Roy, Pergamon Press, New York, pp. 367, 1968.
- [12] Timoshenko S. and Woinowsky-Krieger S., *Theory of Plates and Shells*, 2nd ed., McGraw-Hill, Inc., New York, pp. 56, 1959.